Accepted Manuscript

Physically short crack propagation in metals during high cycle fatigue

C. Santus, D. Taylor

PII: S0142-1123(09)00092-9
DOI: 10.1016/j.ijfatigue.2009.03.002
Reference: JIJF 2248

To appear in: *International Journal of Fatigue*

Received Date: 25 February 2008
Revised Date: 28 January 2009
Accepted Date: 2 March 2009

Please cite this article as: Santus, C., Taylor, D., Physically short crack propagation in metals during high cycle fatigue, *International Journal of Fatigue* (2009), doi: 10.1016/j.ijfatigue.2009.03.002

Physically short crack propagation in metals during high cycle fatigue

C. Santus [a,*] D. Taylor [b]

[a]*Dipartimento di Ingegneria Meccanica, Nucleare e della Produzione. Università di Pisa. Via Diotisalvi n°2 - 56126 - Pisa. Italy.*

[b]*Department of Mechanical Engineering, Trinity College, Dublin 2, Ireland.*

Abstract

In metals, during high cycle fatigue on plain specimens, almost the entire fatigue life is spent as *short* crack initiation and propagation. The fatigue short crack life can be schematically divided into two subsequent phases: *microstructurally* short crack and *physically* short crack. Recently, Chapetti proposed a physically short crack threshold and propagation driving force model [1]. In his model the physically short crack behavior is obtained from the long crack propagation, just introducing the reduced threshold due to unsaturated closure. In the present paper the physically short crack propagation is similarly modeled by means of a driving force equation, but independent from the long crack propagation. In this way, a better description of the short crack behavior is provided, however short crack propagation data is required. Physically short crack propagation model parameters were obtained, by fitting experimental data drawn from the literature, for two Aluminum alloys and a Titanium alloy at two different heat treatment conditions and load ratios.
By calculating the physically short crack plus long crack propagation, and assuming microstructurally short crack as part of the *initiation* stage, a purer information about crack initiation can be drawn from the $S-N$ curves, and it is shown in the paper for the investigated materials. A precise crack initiation size and the number of cycles just for initiation are then provided. This information is useful to accurately predict fatigue life for blunt notched and for thick components, where the propagation is much higher than in the small plain specimen.
A validation of the model was obtained by predicting the fatigue life of a notched specimen. An accurate prediction was obtained both when the initiation was much smaller than propagation and when almost the entire fatigue life was initiation.

Key words: Microstructurally short cracks. Physically short cracks. Fatigue crack initiation. Fatigue crack propagation. Notched component fatigue life.

* Corresponding author:
Phone: +39 050 836607, Fax: +39 050 836665.
Email address: ciro.santus@ing.unipi.it (C. Santus).

Notation

σ_a	Stress amplitude.
$\Delta\sigma$	Stress range ($= 2\sigma_a$).
ΔK	Stress intensity factor range (full range, even for negative load ratio).
ΔK_{th}	Long crack threshold stress intensity factor range.
$\Delta\sigma_{th}$	Threshold stress range.
da/dN	Crack propagation rate.
a	Semielliptical surface crack depth.
w	Semielliptical surface crack width.
σ_0	plain specimen fatigue strength amplitude at high number of cycles to failure.
$\Delta\sigma_0$	plain specimen fatigue strength range ($= 2\sigma_0$).
N_f	Number of cycles to failure.
N_0	Number of cycles to failure at which the fatigue strength σ_0 is based on.
N_i	Number of cycles for initiation.
N_p	Number of cycles for propagation.
C_P	Paris law constant.
m_P	Paris law exponent.
σ_f', b	Basquin's law parameters.
β	Shape factor for crack stress intensity factor.
D_s	Specimen diameter.
$\Delta K_{th,a}$	Crack size dependent physically short crack threshold.
$\Delta K_{th,d}$	Smallest physically short crack threshold.
ΔK_C	Stress intensity range threshold closure term.
k	Exponential factor in Chapetti model.
a_0	Critical distance.
a_D	Critical defect size.
d	Material microstructurally strongest barrier or largest non damaging crack.
d_2	Smallest long crack.
r_n	Notch radius
D_n	Notch depth
d_n	Notch inner diameter.
k_t	Notch stress concentration factor.

1 Introduction

The fatigue strength of metal components without any pre–existing crack or detectable defect has to be explained by the *short* crack mechanisms. After the nucleation the fatigue crack is obviously short. While a crack is short the non propagating condition $\Delta K < \Delta K_{\text{th}}$ could be satisfied even for very high cyclic stress $\Delta\sigma$, much larger than actual values that cause fatigue failure. In other words the Linear Elastic Fracture Mechanics (LEFM) fundamental parameter K loses its meaning while the crack is shorter than some characteristic material length.
There is more than one type of short crack [2]. A fatigue crack that nucleates from an approximately flat surface (such as a plain specimen, or a blunt notch), in ambient air and room temperature, grows through three phases [3]:

- *Microstructurally* Short Crack (MSC), where the continuum mechanics itself is questionable, since the crack size is similar to the grain size, or less;
- *Physically* Short Crack (PSC), where crack growth is increased due to reduced crack closure and other effects;
- *Long* Crack (LC), where Paris law holds, up to the final fracture.

Large scientific literature exists on mechanistic descriptions of MSC and PSC. Main contributions were given by Miller [4,5], Miller and O'Donnell [6], Riemelmoser and Pippan [7], and finally a very clear description of the plasticity induced crack closure mechanisms are available in Pippan and Riemelmoser [8] (crack plastic wake closure mechanism under plane strain conditions) and Pippan et al. [9] (asymmetric crack plastic wake as the reason for roughness induced closure). The lack of fully developed closure is broadly accepted to be the main mechanistic reason for the physically short crack's faster growth. Recently, Chapetti proposed a PSC propagation model based on the reduced closure concept [1]. In the present paper the physically short crack propagation Chapetti model is followed, however some modifications / improvements are provided and motivated.
Usually, the crack initiation is assumed as the existence of a detectable crack size that depends on the inspection technique. Obviously, this definition has a valid experimental meaning. In his recent paper Chapetti suggested as initiation / propagation boundary the transition from MSC to PSC. Indeed, the ΔK is basically meaningless for the fatigue crack in the MSC regime, while it already has a mechanistic soundness in the PSC regime. In the present paper the MSC to PSC crack initiation is quantitatively obtained from the $S-N$ curves by subtracting the PSC and LC propagation portions from the entire fatigue life, and the PSC propagation is obtained integrating the proposed equation.

2 Materials

Materials investigated in the present paper, are aluminum alloys: 2024–T3, 7075–T6 and titanium alloy $(\alpha+\beta)$ Ti–6Al–4V. $S-N$ curves were drawn from Boller

and Seeger materials data book under cyclic loading [10], for load ratio $R=-1$. For the Titanium alloy the load ratio $R=0.1$ is also considered. Data for Ti–6Al–4V alloy loaded at $R=0.1$ are from Peters et al. [11].
The main material properties are reported in Tab.1.

Alloy	S_{Y} MPa	S_{UTS} MPa	R	σ_{f}' MPa	b	N_0	σ_0 MPa	Ref.
2024–T3	378	486	-1	1 044	-0.114	5×10^6	166	[10]
7075–T6	512	572	-1	776	-0.095	5×10^6	168	[10]
Ti–6Al–4V	1 188	1 236	-1	1 797	-0.085	5×10^6	457	[10]
Ti–6Al–4V	915	965	0.1	429	-0.0325	10^8	230	[11]

Table 1
Static and fatigue material properties.

where: S_{Y} is the static Yield strength, S_{UTS} is the Ultimate Tensile Strength, σ_{f}' and b are the two constants defining Basquin's relationship: $\sigma_{\mathrm{a}}=\sigma_{\mathrm{f}}'(2N_{\mathrm{f}})^b$, and σ_0 is the fatigue strength amplitude (i.e. half the full range: $\Delta\sigma_0=2\,\sigma_0$) based on a reasonably high number of cycles to failure N_0 (higher than 10^6).
Even though compositions of Ti–6Al–4V reported in Ref.[10] and Ref.[11] are very similar, the mechanical properties of the two Ti alloys were quite different (higher strength for the alloy reported in Ref.[10]). Apparently, different heat treatments induced different microstructures and then different mechanical properties. To distinguish the two different Titanium alloys in the present paper, the load ratio R is mentioned since alloy from Ref.[10] was loaded at $R=-1$, while alloy from Ref.[11] was loaded at $R=0.1$.

3 Long crack propagation models

Long crack propagation rate can be described accurately by the Paris law, where two material parameters are required only: C_{P} and m_{P}, to be deduced by fitting to experimental data. Several generalizations of the Paris law are available in the literature, that can be easily found in textbooks, e.g. Ref.[12]. Most of them are derived to allow for a unique set of material parameters to take into account load ratio R sensitivity. Other generalizations of the Paris law are designed to model the smooth transition at the near threshold condition. Several models are available, see for example the advanced textbook by Ellyin [13]. However, the two most popular ones assume as an effective parameter the difference between the stress intensity factor range and the threshold stress intensity factor range, but in a slightly different way:

- Zheng and Hirt [14]

$$\frac{\mathrm{d}a}{\mathrm{d}N}=C_{\mathrm{P}}(\Delta K-\Delta K_{\mathrm{th}})^{m_{\mathrm{P}}} \tag{1}$$

• Klesnil and Lukáš [15]

$$\frac{\mathrm{d}a}{\mathrm{d}N} = C_{\mathrm{P}}(\Delta K^{m_{\mathrm{P}}} - \Delta K_{\mathrm{th}}{}^{m_{\mathrm{P}}}) \tag{2}$$

Mechanistic explanations for Eqs.1 and 2 may be questionable and discussion about their validity can be found in many papers, however, even the Paris law finds its main justification just in its fitting experimental data success. Eqs.1 and 2 agree in terms of asymptotes: they give rise to the same threshold and the same crack propagation rate at high driving force $\Delta K \gg \Delta K_{\mathrm{th}}$ but in the intermediate region they differ significantly, since $C_{\mathrm{P}}(\Delta K - \Delta K_{\mathrm{th}})^{m_{\mathrm{P}}} < C_{\mathrm{P}}(\Delta K^{m_{\mathrm{P}}} - \Delta K_{\mathrm{th}}{}^{m_{\mathrm{P}}})$.

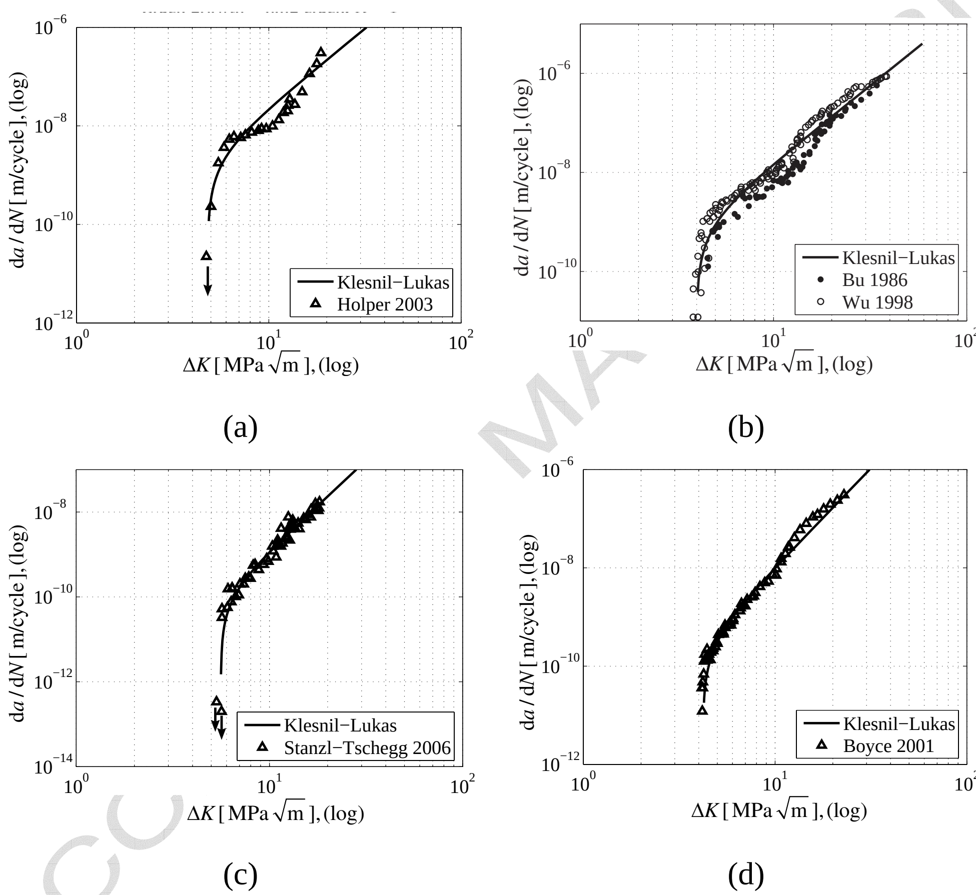

Fig. 1. Long crack near threshold propagation: (a) 2024–T3 ($R = -1$), experimental data from Ref.[16]. (b) 7075–T6 ($R = -1$), Ref.[17,18]. (c) Ti–6Al–4V ($R = -1$), Ref.[19]. (d) Ti–6Al–4V ($R = 0.1$), Ref.[20]. Predictions using the Klesnil–Lukáš approach (Eq.2).

Eq.2 was fitted to the data, drawn from the literature, for the materials mentioned above, and it is reported in Fig.1 where it is clearly effective in describing the near threshold propagation (Eq.2 is termed as “Klesnil–Lukas” in Fig.1). Eq.2 parameters, obtained by fitting materials data just shown, are reported in Tab.2.

From Fig.1 it is clear that Eq.2 offers a good description of the near threshold region, since it captures experimental data quite well for all materials. Eq.1 gave poorer predictions in all cases (not shown here).

Alloy	R	ΔK_{th} $\mathrm{MPa}\sqrt{\mathrm{m}}$	m_{P}	C_{P} $\frac{\mathrm{m/cycle}}{(\mathrm{MPa}\sqrt{\mathrm{m}})^{m_{\mathrm{P}}}}$	Ref.
2024–T3	-1	4.8	3.20	1.5×10^{-11}	[16]
7075–T6	-1	4.0	3.14	1.1×10^{-11}	[17,18]
Ti–6Al–4V	-1	5.6	4.26	6.7×10^{-14}	[19]
Ti–6Al–4V	0.1	4.2	4.05	9.0×10^{-13}	[20]

Table 2
Eq.2 fitting parameters for considered materials.

4 Short crack threshold models

The most effective tool to describe the short crack threshold is the Kitagawa–Takahashi (KT) diagram, Fig.2.

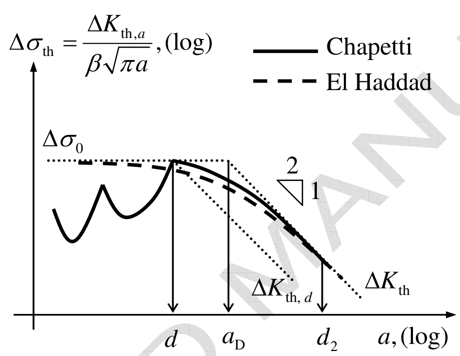

Fig. 2. Kitagawa–Takahashi diagram. El Haddad [21] and Chapetti [1] short to long crack threshold models.

There are some models available to describe the shape of the KT diagram. Among them the El Haddad model is both accurate and simple. Indeed, it just requires the two asymptotes: $\Delta\sigma_0$ and ΔK_{th} as material parameters.

$$\Delta K_{\mathrm{th},a} = \Delta K_{\mathrm{th}}\sqrt{\frac{a}{a+a_{\mathrm{D}}}} \tag{3}$$

where a_{D} is the size of the critical defect:

$$a_{\mathrm{D}} = \frac{a_0}{\beta^2} \tag{4}$$

and a_0 is the material critical distance:

$$a_0 = \frac{1}{\pi}\left(\frac{\Delta K_{\mathrm{th}}}{\Delta\sigma_0}\right)^2 \tag{5}$$

Actually, the El Haddad model was originally formulated using a_0 in Eqs.3 instead of the critical defect size a_{D} [21]. The introduction of a_{D} is explained by considering a self similar fatigue crack which keeps its aspect ratio during propagation.

Then the long crack asymptote in the KT diagram is shifted, due to the shape factor β, which in turn gives the intersection, with the fatigue strength $\Delta\sigma_0$, in a_{D}. A deeper discussion about the meaning of a_{D}, and its relation to a_0, can be referred to Refs.[22,23].

During early fatigue crack propagation, at a plain specimen surface (and at a blunt notch surface too) crack dimensions are much smaller than surface curvature radius and specimen (or component) thickness. It is a reasonable assumption to consider a crack that nucleates from a flat surface in a semi-infinite body, with the crack orientation perpendicular to the uniaxial normal stress direction. In such a situation the typical observed surface crack aspect ratio is $a/w = 0.8$, where a is the crack depth and w is the crack surface half-length. During fatigue crack initial propagation, its aspect ratio can be either higher or lower than 0.8. In particular for sub–surface initiations the crack aspect ratio can temporarily be larger than unity [24], anyway an average aspect ratio $a/w = 0.8$ can be assumed. For this basic crack geometry configuration, the stress intensity factor K at the deepest point of the crack is [25]:

$$\Delta K = \beta \Delta\sigma \sqrt{\pi a}, \quad \beta = 0.746 \tag{6}$$

When the fatigue crack grows and its dimensions become comparable with any significant specimen (or component) geometry dimension, the shape factor β changes. Despite this geometry shape factor sensitivity, the surface crack starting from a semi-infinite body flat surface is here considered as reference geometry, then shape factor $\beta = 0.746$ is also assumed in Eq.4.

The El Haddad model does not explain the different regimes of short cracks, because it is a unique equation that covers the entire scale of crack size. On the contrary, the Chapetti model [1] distinguishes between microstructurally and physically short crack regimes. It considers a transition size d (material dependent only) which is the strongest microstructural barrier of the material. Any crack smaller than d is microstructurally short and its behavior can not be modeled by means of the stress intensity factor. Any crack larger than d is initially physically short, until its closure is saturated as it grows. However, the stress intensity factor can be already used to predict PSC crack propagation rates, provided that the Paris law is modified to consider the reduced closure and the resulting higher propagation rate. Chapetti proposed the following model, to define threshold stress intensity factor range for PSC:

$$\Delta K_{\mathrm{th},a} = \Delta K_{\mathrm{th},d} + \Delta K_{\mathrm{C}} \tag{7}$$

where $\Delta K_{\mathrm{th},d}$ is the smallest physically short crack threshold ($a = d$):

$$\Delta K_{\mathrm{th},d} = \beta \Delta\sigma_0 \sqrt{\pi d} \tag{8}$$

and ΔK_{C} is the closure term:

$$\Delta K_{\mathrm{C}} = (\Delta K_{\mathrm{th}} - \Delta K_{\mathrm{th},d})(1 - e^{-k(a-d)}) \tag{9}$$

in which k is a material constant and a good estimate of it is given by the equation:

$$k = \frac{1}{4d} \frac{\Delta K_{\mathrm{th},d}}{\Delta K_{\mathrm{th}} - \Delta K_{\mathrm{th},d}} \tag{10}$$

Obviously ΔK_{C} is null as $a = d$, and $\Delta K_{\mathrm{th},a}$ tends to the LC threshold ΔK_{th} when a is much larger than d.
As already pointed out, the Chapetti model (Eqs.7–10) is not valid in the MSC region; the resistance curve shown in the MSC region in Fig.2 is qualitative only. The Chapetti model requires a material length d, that should be obtained by means of microstructure observation. The microstructure length d has been observed to be either the average grain size or any microstructural barrier spacing, depending on the material microstructure. For example, d is the ferrite grain size in ferrite-perlite microstructure, or laths spacing in bainite-mertensite steels [1,26], or primary α phase size in bimodal Ti–6Al–4V alloy [27].
The concept of largest non propagating crack was initially introduced several years ago by Taylor and Knott [28]. If a crack shorter than the largest non propagating crack is present in a plain specimen it does not reduce the fatigue strength. Clearly from Fig.2 it follows that the largest non propagating crack is coincident to the Chapetti model's strongest barrier d.
Comparing the Chapetti and El Haddad threshold models, it follows that the El Haddad one is not able to predict the existence of any non damaging crack, though the two lines remain very close.
Values of material lengths d, a_0, a_{D}, drawn from the literature, are reported in Tab.3.

Material	d mm	a_0 mm	a_D mm	Ref.
2024–T3 ($R = -1$)	0.027	0.066	0.111	[1]
7075–T6 ($R = -1$)	0.018	0.045	0.076	[29]
Ti–6Al–4V ($R = -1$)	0.010	0.012	0.020	[30]
Ti–6Al–4V ($R = 0.1$)	0.020	0.027	0.044	[1]

Table 3
Materials characteristic lengths.

The material length d is the grain size for the two aluminum alloys, while d is the primary α phase size for the bimodal Ti alloy. Critical distance a_0 was obtained from data reported in Tabs.1,2, and Eq.5. To obtain a_{D}, from critical distance a_0, the shape factor $\beta = 0.746$ was assumed, as discussed above.
Materials KT diagrams are reported in Fig.3, for the considered materials, and the characteristic lengths are marked on the graphs.
A further material length, shown on the KT diagrams, is the smallest long crack d_2. Both the two models here compared show a smooth transition at d_2 and then they meet the LC threshold. For all the materials investigated in the paper a good estimate of d_2 is: $d_2 = 10\,d$, also in agreement with Taylor and Knott paper [28]. In the present paper this estimate will be considered throughout.

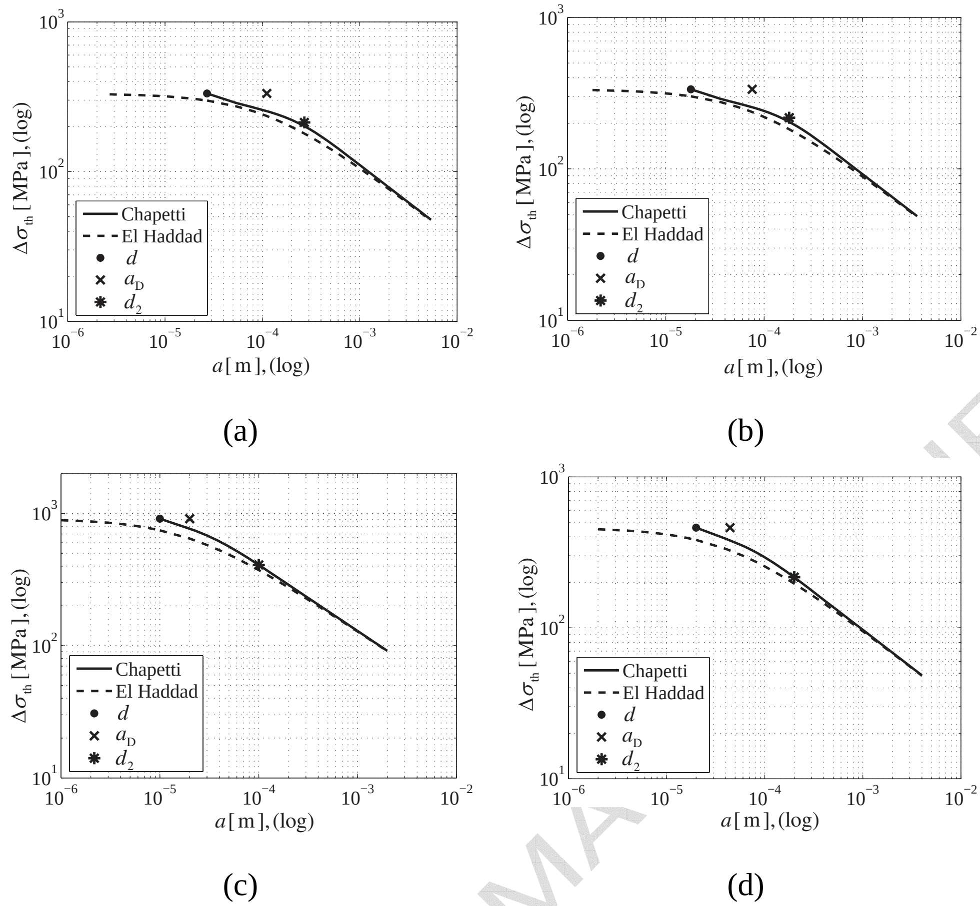

Fig. 3. Kitagawa–Takahashi diagrams and characteristic lengths: d, a_D, d_2, for investigated materials: (a) 2024–T3, $R=-1$. (b) 7075–T6, $R=-1$. (c) Ti–6Al–4V, $R=-1$. (d) Ti–6Al–4V, $R=0.1$.

The Chapetti model threshold stress range is slightly higher the El Haddad prediction. This is particularly true for both the two Ti alloys where a_D is around twice d. The condition of a_D not much larger than d has to be interpreted as little stress intensity factor closure component ΔK_C. For the Ti alloy loaded at load ratio $R=0.1$ the small amount of closure can be addressed to the high load ratio itself, while for the Ti alloy loaded at load ratio $R=-1$, the reason can be the very high yield strength S_Y, Tab.1, which in turn reduces the wake mechanisms responsible for the crack closure [8,9]. For the two aluminum alloys the critical defect size a_D ranges from 3 to 4 times the material microstructural size d.

5 Physically short crack propagation model

To model the PSC propagation rate, Chapetti considered the use of Eq.1, in which he replaced the *long crack* threshold stress intensity factor range ΔK_{th} with the *short crack* threshold $\Delta K_{th,a}$ (defined in Eq.7) that is a function of the crack size a. The crack propagation driving force parameter is the difference between the stress intensity factor range and the threshold stress intensity factor range. Following this

approach the stress intensity full range ΔK is considered instead of the positive portion of the range ΔK^+, or the effective portion of the range ΔK_{eff} (positive portion minus opening stress intensity factor) that are suggested in different approaches. The crack closure during a portion of the fatigue cycle is the intrinsic component of the threshold stress intensity range. The threshold stress intensity factor range increases, as the crack grows, due to the closure saturation. The difference between the full range and the threshold term (Eq.1) correctly considers the crack closure and then it is assumed a physically relevant propagation driving force parameter.
However, the same author also proposed the use of the other equation: Eq.2 to model the short crack propagation, in papers Refs.[27,31].
In the present paper long crack propagation is modeled by means of Eq.2, while Eq.1 is used for physically short crack propagation only, introducing the short crack threshold which is a function of the crack size. Eq.1 is then re–issued here to be dedicated uniquely to the PSC propagation:

$$\frac{\mathrm{d}a}{\mathrm{d}N} = C_{\mathrm{S}}(\Delta K - \Delta K_{\mathrm{th},a})^{m_{\mathrm{S}}} \qquad (11)$$

In the following, the term $\Delta K_{\mathrm{th},a}$ is evaluated by means of the El Haddad short crack threshold Eq.3. By considering Chapetti short crack threshold (Eq.7) in Eq.11, instead of El Haddad, negligible difference would result since the two models are quite similar, Fig.2,3. This difference is much smaller than the inherent short crack propagation data scatter. More importantly, modeling the PSC propagation with Eq.2, and substituting the PSC threshold $\Delta K_{\mathrm{th},a}$, limits the PSC propagation rate to be lower than the Paris straight line ($C_{\mathrm{P}}(\Delta K^{m_{\mathrm{P}}} - \Delta K_{\mathrm{th},a}^{m_{\mathrm{P}}}) < C_{\mathrm{P}}\Delta K^{m_{\mathrm{P}}}$), Fig.4, while experimental data shows that the PSC propagation rate can be higher (see data reported later, in Fig.5).

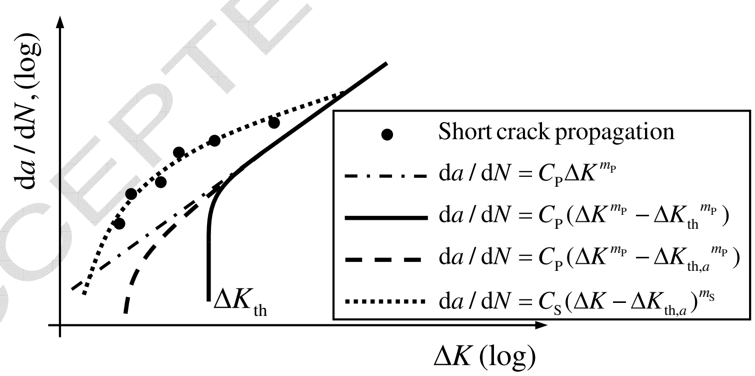

Fig. 4. Crack propagation models.

A similar approach was followed by Navarro et al. in a fretting fatigue application [32]. They found the crack propagation fatigue life portion integrating a growth rate equation proposed by the NASA/FLAGRO software. That equation has a more complex form than the Eq.11, however it contains the term $\Delta K - \Delta K_{\mathrm{th}}$. They introduced the El Haddad short crack correction for ΔK_{th} to obtain higher propagation rate while the crack is short, and then properly model their experimental results.
The short crack propagation rate experimental data are drawn from the literature for all the materials investigated, Fig.5. Eq.11 parameters C_{S} and m_{S} were found by

fitting Eq.11 and results are summarized in Tab.4.

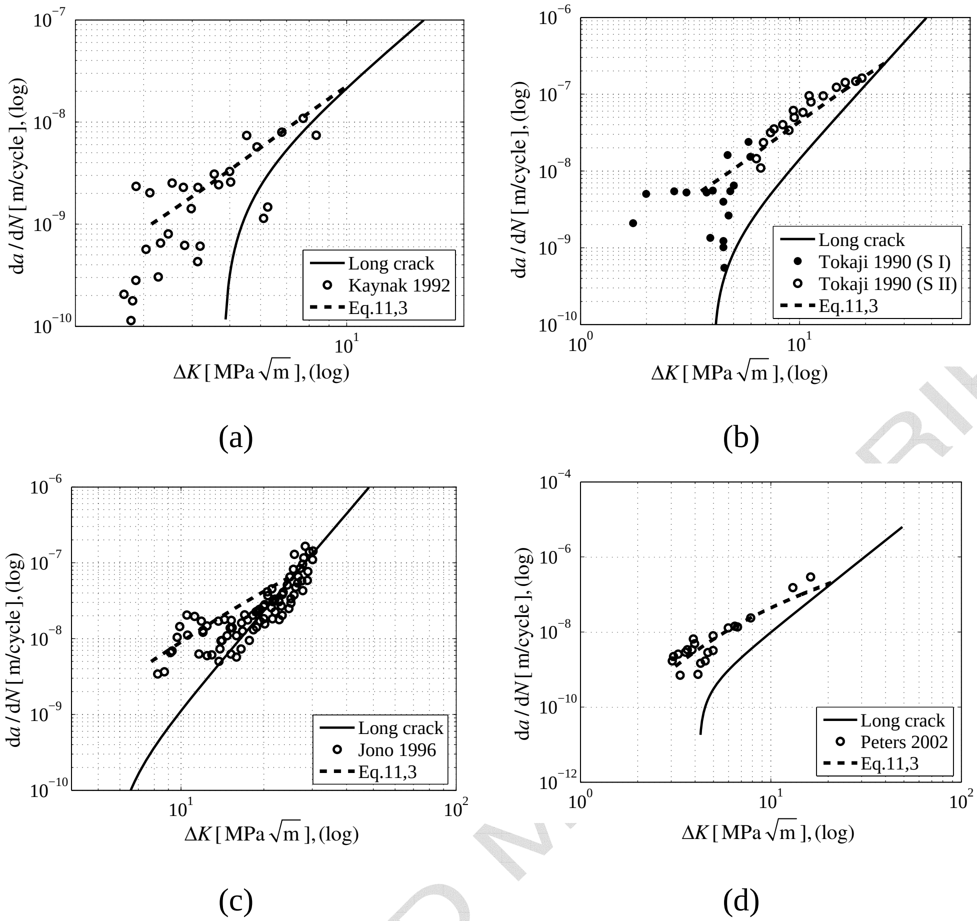

Fig. 5. Short crack propagation prediction given by Eq.11 and El Haddad threshold. (a) 2024–T3, $R = -1$, experimental data from Ref.[33]. (b) 7075–T6, $R = -1$, Ref.[34]. (c) Ti–6Al–4V, $R = -1$, Ref.[35]. (d) Ti–6Al–4V, $R = 0.1$, Ref.[11].

Alloy	R	m_S	C_S $\frac{\text{m/cycle}}{(\text{MPa}\sqrt{\text{m}})^{m_S}}$
2024–T3	-1	1.76	9.75×10^{-10}
7075–T6	-1	1.57	2.20×10^{-9}
Ti–6Al–4V	-1	1.58	6.03×10^{-10}
Ti–6Al–4V	0.1	1.54	2.70×10^{-9}

Table 4
Eq.11 material parameters.

Obviously, it follows that $m_S < m_P$ for all materials. This condition implies that short crack propagation line crosses the long crack propagation line at some crack size. This behavior is well known from short crack propagation experimental observation.

Fig.5(a) reports short crack propagation data for 2024–T3 aluminum alloy [33]. Eq.11 with El Haddad threshold is shown for a short crack a ranging from d to d_2, exactly the physically short crack size range.

Fig.5(b) shows short crack propagation data for 7075–T6 aluminum alloy. In Ref.[34] two series of short crack propagation data are reported at two quite similar cyclic stress ranges, then in the present paper model the average cyclic stress was assumed $\Delta\sigma = 610$ MPa. Moreover, short crack data in Ref.[34] are distinguished between Stage I and Stage II propagation. It is possible to observe that Stage I / Stage II transition is slightly later that MSC / PSC transition, indeed some points in the PSC regime are still in the Stage I propagation. Obviously this result is not general, but it is restricted to this particular alloy at this loading condition. The present paper model (Eq.11, dashed line) was obtained simulating a short crack a ranging from d to $5\,d_2$. The PSC higher rate propagation does not cross the long crack behavior at exactly d_2 but for a larger crack size. Other short crack fatigue data were available in the literature for this (quite common) aluminum alloy. In particular, short crack data reported in Ref.[17], showed a higher rate than long cracks, even at quite large crack size, in the order of millimeters. As discussed above, Eq.11 allows for PSC higher propagation rate than LC even for a crack larger than d_2. However, data reported in Ref.[17] was not completely coherent with the short crack model here obtained, because PSC higher propagation rate than LC was extended to very large crack size.

Fig.5(c) shows short crack propagation data for Ti–6Al–4V ($R = -1$). In Ref.[35] several cyclic stress series are reported, not very different among them. The average cyclic stress $\Delta\sigma = 1271$ MPa was considered and short crack material parameters obtained. In the reported model short crack a ranges from $2d$ to $2\,d_2$. Unfortunately, short crack data are not available in the very short crack threshold region (with at least some points lower than 10^{-9} m/cycle) limiting the accuracy check of the proposed model. For the same material, and loading condition, a very similar prediction was obtained from data in Ref.[36] (for brevity not reported here).

Finally, Fig.5(d) shows short crack propagation data for Ti–6Al–4V ($R = 0.1$). In Ref.[37] short crack propagation data is reported for cyclic stress $\Delta\sigma = 450$ MPa. The reported models were obtained for a short crack a ranging from $1.3\,d$ to $6\,d_2$. For this material and loading condition, the short / long crossing point is obtained for $a = 6\,d_2$, i.e. for a crack size which definitely should be already ‘long’. This apparent model inconsistency was already found for materials 7075–T6 and Ti–6Al–4V ($R = -1$). It is worth stressing that the short / long crack size transition for crack *propagation* rate can be much higher than the short / long crack size transition at *threshold* (d_2).

An experimental evidence is that the stress intensity factor does not completely describe the short crack behavior, but the short crack propagation is also sensitive to the stress level $\Delta\sigma$. In other words two short cracks, different in size, but loaded by the same ΔK, do not show same propagation rate; in particular the shorter one grows faster than the other because it is loaded by a higher cyclic stress level. This experimental evidence is acknowledged in the present PSC propagation model Eqs.11,3, indeed the threshold term is sensitive to the crack size. Fig.6(a) shows short crack propagation data, previously presented about the 7075–T6 aluminum alloy, where two data series were produced at different stress levels $\Delta\sigma$ (previously considered as a unique test series) [34]. Eq.11 was calculated with the two different stress levels $\Delta\sigma$ that the experimental series were obtained. At the same ΔK, the higher the stress level, the higher the propagation rate, coherently with the experimental results. However, Fig.6(a) data was obtained with very similar cyclic stress levels and then the two lines are almost overlapped, indeed the two experimental series are very near. A clearer comparison is given by Fig.6(b) that shows same material short crack propagation, under a lower cyclic stress. This other short crack series was drawn from the paper by Bu and Stephens, Ref.[17]. The present model reproduces a slower propagation rate, especially near the threshold, in agreement with the experimental results.

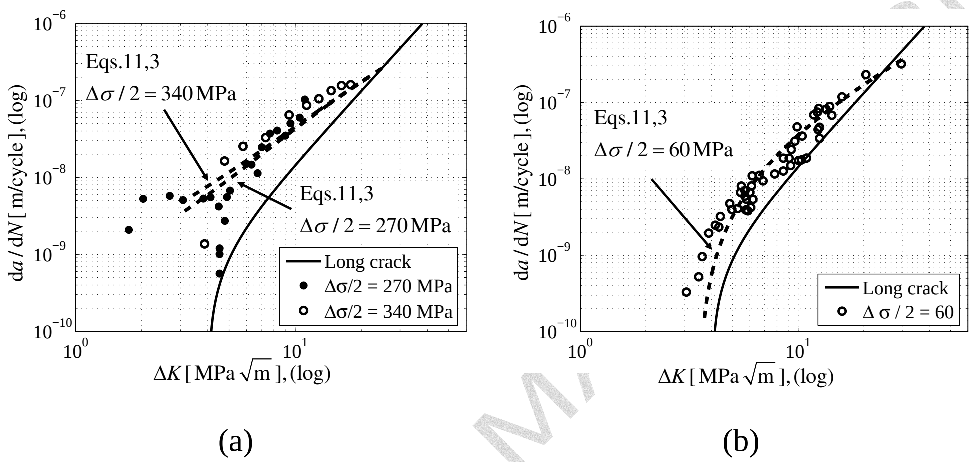

Fig. 6. Short crack propagation sensitivity to load level $\Delta\sigma$: (a) high cyclic stress level, data from Tokaji et al. 1990 [34], (b) low cyclic stress level, data from Bu and Stephens 1986 [17].

In the PSC regime the small scale yielding condition can be at the limit of its validity. For example, assuming the simple Irwin's model to esteem the plastic size for a semielliptical crack ($\beta = 0.748$) with a crack size $a = 0.100$ mm, in a thick 7075–T6 aluminum alloy component (yield strength $S_{\mathrm{Y}} = 500$ MPa), loaded by $\sigma = 300$ MPa, stress intensity factor $K = 4.0$ MPa$\sqrt{\mathrm{m}}$, the plane strain plastic size is $r_{\mathrm{p}} = 0.004$ mm, i.e. 25 times smaller the crack size. Miller [4] pointed out that the small scale yielding condition is valid for a crack size to plastic size ratio at least 50 or higher. So, in the PSC regime the stress level is below the yield limit (otherwise *mechanically* short crack would be the case) but the small scale yielding validity can be not fully satisfied. Therefore, the not saturated crack closure it is not the only reason of physically short crack faster propagation, but also the large crack tip plastic region can play its role. This is here considered the reason of a PSC propagation equation (Eq.11) independent from the long crack propagation equation (Eq.2), while the Chapetti model derived the PSC equation from the LC equation because he considered the not saturated crack closure condition as the unique reason of PSC faster growth.

6 Fatigue crack initiation from *S–N* curves

Finite life HCF testing is usually obtained from plain specimens under cyclic axial load. The number of cycles to failure N_f is considered at the complete fracture of the specimen, or sometimes, at the occurrence of a visible crack, or a crack large enough that reduces specimen stiffness perceptibly. In all these three conditions the final crack size is already long.

Assuming initiation / propagation transition at d crack size, it is possible to predict the number of cycles for propagation and then subtract the propagation portion to find the number of cycles just for initiation. The propagation phase is given by the PSC propagation plus the LC propagation, up to the final failure (or one of the conditions above). To find the number of cycles for PSC propagation it suffices to integrate Eq.11 starting from d up to the short / long crack crossing point. After that, physically short crack becomes long crack and then propagation prediction is given by Eq.2. A purer *initiation* information is then drawn from the $S-N$ curves: the number of cycles N_i to nucleate the d crack size, as function of the cyclic load amplitude σ_a, in the HCF regime.

The idea of subtracting the propagation portion from the $S-N$ curve was also recently proposed by McClung et al., [38]. They did not suggest a precise initiation size, they just proposed a crack size much shorter than 1 mm (which is traditionally considered the initiation from an engineering point of view) but not shorter than the material grain size.

To back calculate the plain specimen crack growth some assumptions were introduced. As the crack propagates through a round specimen bar, the crack shape factor β increases, mainly because the ligament area reduces. The round bar crack through stress intensity factor problem has been widely investigated, even recently, through Finite Element (FE) [39–43,24]. In these papers particular attention was devoted to the crack shape evolution, when the crack propagates inside the round bar, for different initial elliptical crack aspect ratios. While the crack size is equal to (or not much larger than) the material length d, the crack is very smaller than the specimen diameter D_s (usually around 10 mm). This geometrical configuration is equivalent to the semielliptical flat surface crack in a seminfinite body. The aspect ratio evolution, as the crack grows inside the specimen, is not considered in the present paper because almost the entire propagation is spent as the crack is much smaller than D_s. The initial preferential aspect ratio $a/c = 0.8$ is assumed throughout the entire life of the fatigue crack. However, the dependency of the shape factor β to a/D_s (assuming constant aspect ratio), has been taken into account following the results published in Ref.[39].

In Fig.7 the propagation portion N_p is compared to the entire fatigue life N_f and the initiation portion N_i results as difference. The HCF *initiation* $S-N$ curves were found for all the investigated materials.

It is evident that the despite materials scatter, the predicted propagation life was always lower than the entire fatigue life for all materials, in the HCF regime $N_f > 10^4$. Among the four investigated materials, the Ti alloy loaded at $R = 0.1$ shows a much lower propagation fraction, and then almost the entire fatigue life is initiation, even for high stress levels.

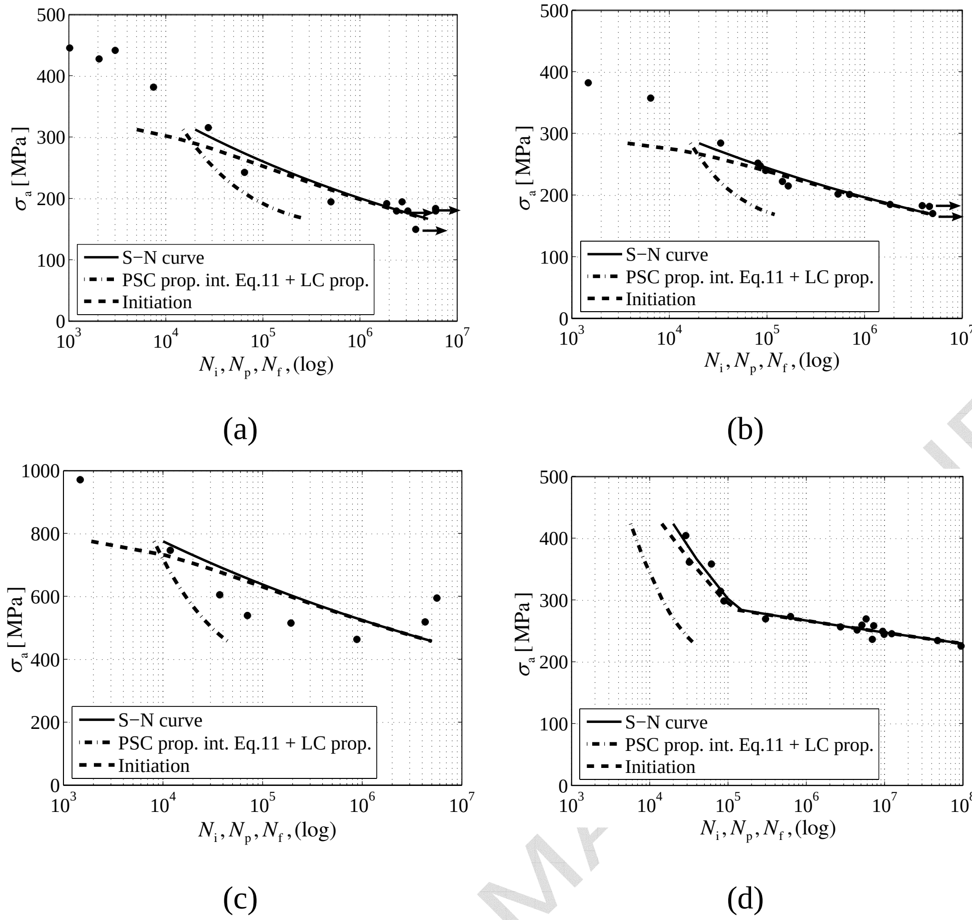

Fig. 7. Predicted propagation fatigue life portion, against entire fatigue life: (a) 2024–T3, $R = -1$, fatigue data is from Ref.[10]. (b) 7075–T6, $R = -1$, Ref.[10]. (c) Ti–6Al–4V, $R = -1$, Ref.[10]. (d) Ti–6Al–4V, $R = 0.1$, Ref.[11].

7 Application

In a notched component the fatigue crack propagation is a large portion of the entire fatigue life. The stress at the notch root is high, then the fatigue crack easily initiates, but as the crack grows the stress intensity factor trend is lower than in the plain specimen geometry, due to the stress gradient. The crack propagation emanating from a notch can experience a retardation or the crack can even stop propagating. The present model focuses on the *physically* short crack only, the mechanically short crack fatigue life can not be predicted with the proposed model. A finite radius notch specimen fatigue $S-N$ curve was considered to validate the model. MacGregor and Grossmann [44,12] published un–notched and notched fatigue data for the main aeronautical structural materials. In particular they published aluminum alloy 2024–T4 round notched fatigue test results, with notch depth $D_\mathrm{n} = 1.59$ mm, notch inner diameter $d_\mathrm{n} = 7.62$ mm, and notch radius $r_\mathrm{n} = 0.25$ mm, Fig.8(a). In the present paper, the literature data was found for the aluminum alloy 2024–T3. The T4 heat treatment means no plastic deformation during the treatment, while the T3 heat treatment means plastic deformation before the aging. Though the slightly different heat treatments the two materials showed very similar mechanical properties,

indeed the plain specimen $S-N$ fatigue curve, reported by MacGregor and Grossmann [44] (not reported here for brevity) and the $S-N$ curve reported by Boller and Seeger showed very similar mean lines.
The crack initiation number of cycles can be obtained from the material *initiation* $S-N$ curve that was found in the previous section, Fig.7(a). At the blunt notch root the stress distribution is approximately uniaxial and uniform, up to a depth equal to d, so in similar conditions than that reproduced by the plain specimen $S-N$ testing, Fig.8(b). After the initiation, the subsequent PSC plus LC propagation phases were evaluated by assuming a semielliptical crack growing from the notch root, calculating the stress intensity factor at the deepest point on the crack front and using the proposed propagation model. FE simulations were performed to calculate the stress intensity factor for different crack sizes. A solid three–dimensional analysis was performed first, followed by a plane strain analysis submodel simulation [45], obtaining the stress intensity factor using the parabolic quarter–point elements [25]. A numerical fit was then used to find the stress intensity factor as a function of the crack size.

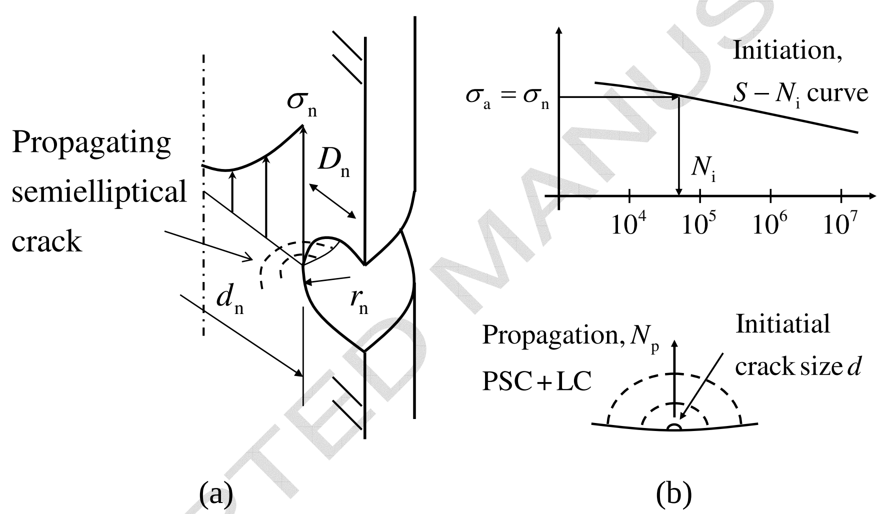

Fig. 8. Blunt notch under fatigue loading: (a) geometry, (b) fatigue crack initiation and propagation predictions.

The comparison between the experimental and the model prediction results are reported in Fig.9(a). The notched specimen initiation curve was obtained from the plain specimen initiation curve, divided by the notch stress concentration factor k_t. The initiation stress range divided the notched tests into three groups: the tests above the initiation stress range (from the highest stress test, labeled 'H', to the test labeled 'P'); the tests inside the initiation range (from test 'I' to 'D'); and finally the test 'R' below the initiation stress range, Fig.9(a).
The prediction of the first group of tests was propagation only, because the initiation is small in comparison to the PSC and LC propagation. For each test the predicted fatigue life was very similar to the experimental, Fig.9(a).
The prediction of the second group was initiation plus propagation. Again the experimental results were accurately reproduced by the prediction, see for example test 'A'. However, the model overestimated the fatigue life of test 'B', and failed to predict tests 'C' and 'D'. Fig.9(b) shows the short crack stress intensity factor

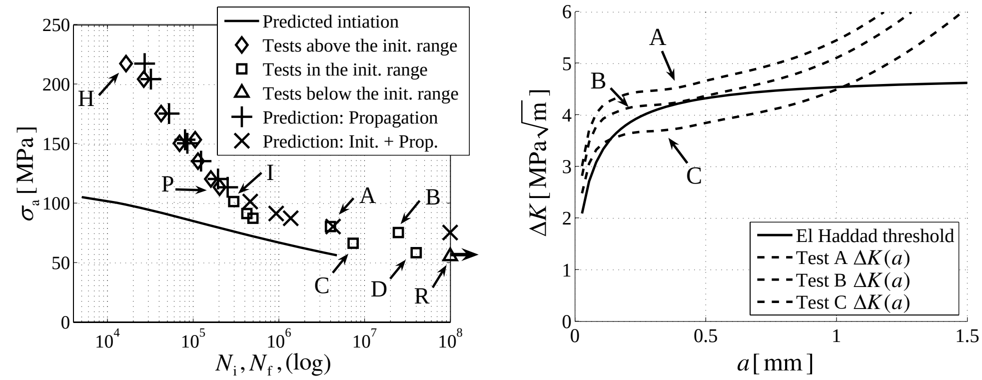

(a) (b)

Fig. 9. Notched geometry results: (a) prediction fatigue life compared with the experimental results, (b) non propagating crack prediction.

range as function of the crack size at the notch root $\Delta K(a)$, and the El Haddad resistance curve $\Delta K_{\mathrm{th},a}$, Eq.3. The driving force is the difference of the two, according to Eq.11. In test 'A', the short crack experiences a retardation but does not stop. In test 'B', the $\Delta K(a)$ curve almost collapses on the resistance curve, and then the predicted propagation is very high, due to the strong retardation at the crack size where two curves are very near. This critical condition is very sensitive to many factors that are here approximated, such as the actual resistance curve, and also the crack aspect ratio that is here assumed $a/c = 0.8$ as in the plain specimen, but that can be smaller for a notch crack, and then the $\Delta K(a)$ would be higher. About the tests 'C' and 'D', after the initiation, the model predicts the non propagating condition when the $\Delta K(a)$ curve crosses the El Haddad resistance curve. On the contrary, the experimental evidence is failure instead of crack arrest. It is difficult to provide a precise explanation of this, because again many factors can play a role. A possible mechanism of coalescence of multiple initiated cracks can generate a wide crack front. The actual ΔK would be quite higher than that predicted assuming a single crack leading to propagation up to the final failure, instead of crack arrest.
Finally, the test 'R' was predicted as not initiated crack, because the stress level was below the initiation stress range, indeed, it was a run out test.

8 Discussion

This study offers a link between fatigue stress and fatigue fracture mechanics approaches. The stress approach can be used to predict the number of cycles just for initiation, and a precise initial propagation crack size is given. After that, the fracture mechanics can be used and the entire fatigue life obtained. This initiation / propagation separation is useful especially when the propagation phase is expected to be larger than that in the $S-N$ plain specimen tests. If the fatigued component is thick the propagation phase is much longer than during small plain specimen testing. An other example of application of the present paper procedure is a blunt notched component, as the validation case presented in the Application. If the plain and the notched specimens are compared in terms of the peak stress at the notch root (σ_n in Fig.8) the notched component fatigue strength would be underestimated. This is usually expressed by the fact that the fatigue notch factor is lower than the stress concentration factor. However, the information given by the plain specimen fatigue $S-N$ curve and the material short crack propagation allowed to reproduce notched fatigue strength calculating the initiation and the further propagation, taking into account the stress gradient below the notch root surface. In principle, this approach is an extension of the Theory of Critical Distances, because a generic notched geometry fatigue strength is obtained combining the two material pieces of information drawn from the two extreme conditions: the fatigue strength of the *plain* specimen: no stress concentration; and the fatigue behavior of the *crack*: strongest stress concentration.

In the paper, the short crack propagation materials data and the $S-N$ curves were drawn from independent testing for all investigated alloys, except for Ti alloy Ti–6Al–4V, $R = 0.1$. Some inaccuracy of the results here shown, can be ascribed to the fact that crack propagation and fatigue life were drawn from just nominally same materials. In the Application case study, the discrepancy between the model prediction and the experimental finite fatigue life for tests 'C' and 'D' (Fig.9) can also be addressed to the not perfectly equal materials heat treatments, especially in the critical condition of almost arrested crack, where the model discrepancy was higher. It was also found (details are not reported for brevity) that the aspect ratio plays a very important role especially if a small difference of the predicted stress intensity factor generates large difference of the predicted propagation number of cycles, or even discriminates the propagating or arrest condition. However, the errors in predicting specimens B, C and D are quite small and fall within the scatter in the experimental results.

The size of the microstructure strongest barrier should be determined from the crack growth rate data, while it is here suggested to esteem d from the material microstructure direct observation, looking for different metallic microstructure features depending on the alloy and heat treatment. Obtaining d from the material observation it is simpler than from crack growth rate and it is enough accurate to provide an indicative length that can be used in the proposed model.

The present physically short crack model can also be used for extending damage tolerant approach. If the experimental crack inspection resolution is adequate to detect cracks in the physically short crack regime, the remaining fatigue life can be calculating, offering larger inspection periods.

9 Conclusions

(1) A physically short crack model was proposed, based on the driving force concept. Materials parameters were obtained by fitting experimental data drawn from the literature.

(2) The present approach differentiates from Chapetti model by considering physically short crack propagation driving force equation independent from long crack propagation. Indeed, physically short cracks can show higher propaga-

tion rate, than expected according to long crack behavior, even when the crack size is already quite larger than the minimum long crack threshold size. The proposed model does not explain the mechanistic reason for that, but it offers a phenomenological tool to describe this behavior. Moreover, El Haddad threshold was assumed instead of Chapetti threshold. El Haddad equation is simpler and the values are quite similar.

(3) By subtracting physically short, and long, crack propagation cycles from the entire fatigue life, it is then possible to extract the initiation number of cycles from the $S-N$ curves.

(4) Aluminum alloys 2024–T3, 7075–T6 and Ti alloy Ti–6Al–4V $S-N$ curves, load ratio $R=-1$, showed that propagation portion is actually negligible approaching to the fatigue strength, but near $N_\mathrm{f}=10^4$ propagation is already a large portion of the entire fatigue life. On the contrary, Ti alloy Ti–6Al–4V, load ratio $R=0.1$, showed physically short crack rate so high that even at $N_\mathrm{f}=10^4$ propagation is still a small portion of the entire fatigue life.

(5) A validation of the model was provided by predicting the fatigue $S-N$ curve of a notched specimen and comparing the calculated fatigue life to the experimental result. The model was able to predict the number of cycles to failure quite accurately both when the initiation was smaller than the propagation and when the initiation was predominant.

References

[1] M.D. Chapetti. Fatigue propagation threshold of short cracks under constant amplitude loading. *International Journal of Fatigue*, 25(12):1319–1326, 2003.

[2] S. Suresh. *Fatigue of Materials*. Cambridge University Press, 2nd edition, 1998.

[3] S. Suresh and R.O. Ritchie. The Propagation of Short Fatigue Cracks. *International Metals Reviews*, 29(6):445–476, 1984.

[4] K.J. Miller. The short crack problem. *Fatigue & Fracture of Engineering Materials & Structures*, 5(3):223–232, 1982.

[5] K.J. Miller. The two thresholds of fatigue behaviour. *Fatigue & Fracture of Engineering Materials & Structures*, 16(9):931–939, 1993.

[6] K.J. Miller and W.J. O'Donnell. The fatigue limit and its elimination. *Fatigue & Fracture of Engineering Materials & Structures*, 22(7):545–557, 1999.

[7] F.O. Riemelmoser and R. Pippan. Consideration of the mechanical behaviour of small fatigue cracks. *International Journal of Fracture*, 118(3):251–270, 2002.

[8] R. Pippan and F.O. Riemelmoser. Visualization of the plasticity–induced crack closure under plane strain conditions. *Engineering Fracture Mechanics*, 60(3):315–322, 1998.

[9] R. Pippan, G. Strobl, H. Kreuzer, and C. Motz. Asymmetric crack wake plasticity – a reason for roughness induced crack closure. *Acta Materialia*, 52(15):4493–4502, 2004.

[10] C. Boller and T. Seeger. *Materials data for cyclic loading*, volume 42E of *Materials science monographs*. Elsevier, 1987. Part D: Aluminium and titanium alloys.

[11] J.O. Peters, B.L. Boyce, X. Chen, J.M. McNaney, J.W. Hutchinson, and R.O. Ritchie. On the application of the Kitagawa–Takahashi diagram to foreign-object damage and high-cycle fatigue. *Engineering Fracture Mechanics*, 69(13):1425–1446, 2002.

[12] N.E. Dowling. *Mechanical Behavior of Materials: Engineering Methods for Deformation, Fracture, and Fatigue*. Prentice Hall, 3rd edition, 2007.

[13] F. Ellyin. *Fatigue damage, crack growth and life prediction*. Chapmen & Hall, 1st edition, 1997.

[14] X. Zheng and M.A. Hirt. Fatigue crack propagation in steels. *Engineering Fracture Mechanics*, 18(5):965–973, 1983.

[15] M. Klesnil and P. Lukáš. *Fatigue of metallic materials*, volume 7 of *Materials science monograph*. Elsevier, 1980.

[16] B. Holper, H. Mayer, A.K. Vasudevan, and S.E. Stanzl-Tschegg. Near threshold fatigue crack growth in aluminium alloys at low and ultrasonic frequency: Influences of specimen thickness, strain rate, slip behaviour and air humidity. *International Journal of Fatigue*, 25(5):397–411, 2003.

[17] R. Bu and R.I. Stephens. Comparison of short and long fatigue crack growth in 7075–T6 aluminum. *Fatigue & Fracture of Engineering Materials & Structures*, 9(1):35–48, 1986.

[18] X.R. Wu, J.C. Newman, W. Zhao, M.H. Swain, C.F. Ding, and E.P. Phillips. Small crack growth and fatigue life predictions for high-strength aluminium alloys: part I–experimental and fracture mechanics analysis. *Fatigue & Fracture of Engineering Materials & Structures*, 21(11):1289–1306, 1998.

[19] S. Stanzl-Tschegg. Fatigue crack growth and thresholds at ultrasonic frequencies. *International Journal of Fatigue*, 28(11):1456–1464, 2006.

[20] B.L. Boyce and R.O. Ritchie. Effect of load ratio and maximum stress intensity on the fatigue threshold in Ti–6Al–4V. *Engineering Fracture Mechanics*, 68(2):129–147, 2001.

[21] M.H. El Haddad, T.H. Topper, and K.N. Smith. Prediction of non propagating cracks. *Engineering Fracture Mechanics*, 11(3):573–584, 1979.

[22] B. Atzori, P. Lazzarin, and G. Meneghetti. Fracture mechanics and notch sensitivity. *Fatigue & Fracture of Engineering Materials & Structures*, 26(3):257–267, 2003.

[23] D. Taylor. *The theory of critical distances: a new perspective in fracture mechanics*. Elsevier, 2007.

[24] K.O. Findley, S.W. Koh, and A. Saxena. J–integral expressions for semi–elliptical cracks in round bars. *International Journal of Fatigue*, 29(5):822–828, 2007.

[25] T.L. Anderson. *Fracture Mechanics: Fundamentals and Applications*. Taylor & Francis, 3rd edition, 2005.

[26] M.D. Chapetti, T. Tagawa, and T. Miyata. Fatigue notch sensitivity of steel blunt–notched specimens. *Fatigue & Fracture of Engineering Materials & Structures*, 25(2):619–723, 2002.

[27] M.D. Chapetti. Application of a threshold curve model to high-cycle fatigue behavior of small cracks induced by foreign-object damage in Ti–6Al–4V. *International Journal of Fatigue*, 27(5):493–501, 2005.

[28] D. Taylor and J.F. Knott. Fatigue crack propagation behaviour of short cracks; the effect of microstructure. *Fatigue & Fracture of Engineering Materials & Structures*, 4(2):147–155, 1981.

[29] J. Lankford. The growth of small fatigue cracks in 7075–T6 aluminum. *Fatigue & Fracture of Engineering Materials & Structures*, 5(3):233–248, 1982.

[30] T. Ogawa, K. Tokaji, and K. Ohya. The effect of microstructure and fracture surface roughness on fatigue crack propagation in a Ti–6A1–4V alloy. *Fatigue & Fracture of Engineering Materials & Structures*, 16(9):973–982, 1993.

[31] M.D. Chapetti. High–cycle fatigue of austempered ductile iron (ADI). *International Journal of Fatigue*, 29(5):860–868, 2007.

[32] C. Navarro, M. Garcia, and J. Dominguez. A procedure for estimating the total life in fretting fatigue. *Fatigue & Fracture of Engineering Materials & Structures*, 26(5):459–468, 2003.

[33] C. Kaynak and A. Ankara. Short fatigue crack growth in AL 2024–T3 and AL 7075–T6. *Engineering Fracture Mechanics*, 43(5):769–778, 1992.

[34] K. Tokaji, T. Ogawa, and Y. Kameyama. The effects of stress ratio on the growth behaviour of small fatigue cracks in an aluminum alloy 7075–T6 (with special interest in stage i crack growth). *Fatigue & Fracture of Engineering Materials & Structures*, 13(4):411–421, 1990.

[35] M. Jono and A. Sugeta. Crack closure and effect of load variation on small fatigue crack growth behaviour. *Fatigue & Fracture of Engineering Materials & Structures*, 19(2–3):165–174, 1996.

[36] K. Tokaji. High cycle fatigue behaviour of Ti–6Al–4V alloy at elevated temperatures. *Scripta Materialia*, 54(12):2143–2148, 2006.

[37] J.O. Peters and R.O. Ritchie. Foreign-object damage and high-cycle fatigue of Ti–6Al–4V. *Materials Science and Engineering A*, 319–321:597–601, 2001.

[38] R.C. McClung, W.L. Francis, and Jr. S.J. Hudak. A new approach to fatigue life prediction based on nucleation and growth. In Elsevier, editor, *Fatigue 2006 – 9th International Fatigue Congress*, 2006. Atlanta, GA.

[39] A. Carpinteri. Elliptical–arc surface cracks in round bars. *Fatigue & Fracture of Engineering Materials & Structures*, 15(11):1141–1153, 1992.

[40] A. Carpinteri and R. Brighenti. Part-through cracks in round bars under cyclic combined axial and bending loading. *International Journal of Fatigue*, 18(1):33–39, 1996.

[41] Y.S. Shih and J.J. Chen. Analysis of fatigue crack growth on a cracked shaft. *International Journal of Fatigue*, 19(6):477–485, 1997.

[42] C.Q. Cai and C.S. Shin. A normalized area-compliance method for monitoring surface crack development in a cylindrical rod. *International Journal of Fatigue*, 27(7):801–809, 2005.

[43] C.S. Shin and C.Q. Cai. Evaluating fatigue crack propagation properties using a cylindrical rod specimen. *International Journal of Fatigue*, 29(3):397–405, 2007.

[44] C.W. MacGregor and N. Grossman. Effects of Cyclic Loading on Mechanical Behavior of 24S–T4 and 75S–T6 Aluminum Alloys and SAE 4130 Steel. In *National Advisory Commitee for Aeronautics*, 1952. NACA TN 2812.

[45] ANSYS, Inc., Southpointe - 275 Technology Drive Canonsburg, PA 15317 U.S.A. *ANSYS Elements Reference*.